Effect of surface phosphorus functionalities of activated carbons containing oxygen and nitrogen on electrochemical capacitance

ARTICLE *in* CARBON · MAY 2009

Impact Factor: 6.2 · DOI: 10.1016/j.carbon.2009.02.006 · Source: PubMed

7 AUTHORS, INCLUDING:

Mykola Seredych
City College of New York
111 PUBLICATIONS **2,617** CITATIONS
SEE PROFILE

P. E. Stallworth
City University of New York - Hunter College
45 PUBLICATIONS **533** CITATIONS
SEE PROFILE

Steve G. Greenbaum
City University of New York - Hunter College
249 PUBLICATIONS **4,003** CITATIONS
SEE PROFILE

Teresa J Bandosz
City College of New York
373 PUBLICATIONS **10,491** CITATIONS
SEE PROFILE

Published in final edited form as:
Carbon N Y. 2009 May 1; 47(6): 1576–1584. doi:10.1016/j.carbon.2009.02.006.

Effect of surface phosphorus functionalities of activated carbons containing oxygen and nitrogen on electrochemical capacitance

Denisa Hulicova-Jurcakova[b], **Mykola Seredych**[a], **Gao Qing Lu**[b], **N.K.A.C. Kodiweera**[c], **Phillip E. Stallworth**[c], **Steven Greenbaum**[c], and **Teresa J. Bandosz**[a,*]

[a]The City College of New York, Department of Chemistry, 160 Convent Ave., New York, NY 10031, United States

[b]The University of Queensland, ARC Centre of Excellence for Functional Nanomaterials, Australian Institute for Bioengineering and Nanotechnology, Corner College and Cooper Roads, St. Lucia, 4072 QLD, Australia

[c]Hunter College, Department of Physics and Astronomy, 695 Park Ave., New York, NY 10065, United States

Abstract

Micro/mesoporous activated carbons containing oxygen and phosphorus heteroatoms were modified by incorporation of nitrogen using melamine and urea precursors. The surface chemistry was analyzed by the means of elemental analysis, XPS, and ^{31}P MAS NMR. The results indicate that upon the incorporation of nitrogen at high temperatures not only new species involving carbon/nitrogen/oxygen are formed but also the phosphorous environment is significantly altered. Both urea and melamine precursors have similar effects on formation of P–N and P–C bonds. These compounds, although present in small but measurable quantities seem to affect the performance of carbons in electrochemical capacitors. With an increase in the heterogeneity of phosphorus containing species and with a decrease in the content pyrophosphates the capacitance increases and the retention ratio of the capacitor is improved.

1. Introduction

Activated carbons are well known as promising materials for electrochemical capacitors [1, 2]. The specific capacitance of activated carbon falls into the range of 100–400 F/g. In recent years several research groups confirmed that their porous structure and particularly the optimal pore size are the most influential factors determining their capacitive performance in supercapacitor [3–8]. In spite of this agreement the energy storage process on activated carbons is far from full understanding. The problems encountered lie in the complexity of the carbon surfaces. Although activated carbons are known for their developed surface area and high pore volumes, it is very difficult to obtain carbon with homogeneous pore sizes, particularly at an industrial scale.

Apart from the porous structure, activated carbons possess complex surface chemistry, which alters the electrochemical energy storage of carbons. As a result of self-oxidation the carbon surface is usually decorated with oxygen containing functional groups representing compounds such as carboxylic acids, phenols, lactones, carboxylic anhydrates, ketones, ethers, quinones or pyrones [9,10]. Among those, the latter two are considered as basic and the quinone/

*Corresponding author: Fax: +1 212 650 6107. E-mail address: tbandosz@ccny.cuny.edu (T.J. Bandosz).

hydroquinone redox reaction was indicated as responsible for the pseudocapacitance of the carbon materials [11,12]. The previous work also suggested that the pyrone oxygen is electrochemically active [13,14].

Besides oxygen, the most common heteroatom studied from the point of view of its effects on the catalytic [15] and electrochemical performance [16–18] of activated carbons is nitrogen. When nitrogen-rich carbons are synthesized/modified at high temperatures, the majority of nitrogen is present as pyrollic, pyridinic, quaternary or pyridinic-N-oxides [19–21]. Besides negatively charged nitrogen in pyridinic and pyrollic arrangements, which are proposed to take part in pseudocapacitive Faradaic reactions [16,22], quaternary and pyridic-N-oxides, when distributed in the pores accessible to ions, were found as important to enhance the capacitance [13,14].

The objective of this study is to investigate the role of another heteroatom, phosphorus and its compounds on the electrochemical performance of activated carbons. Although phosphorus is not a commonly encountered element in all carbon it is always present in measurable quantity in carbons obtained using phosphoric acid activation [23,24]. A closer look is taken on the surface chemistry of wood based carbons, whose electrochemical performance was described previously [13]. In this study for the first time the chemical environment of phosphorus is investigated in conjunction with oxygen and nitrogen functional groups. In that light, the speciation of nitrogen and oxygen containing groups is revisited and an attempt is made to elucidate the effect of phosphorus on the measured capacitance and capacitance retention ratio. So far the aspect of phosphorus incorporated into the carbon matrix has not been discussed as affecting the performance of carbon electrodes.

2. Experimental

2.1. Materials

Activated carbon of wood origin BAX-1500 (MeadWestvaco) was used in this study. Its surface modifications were described in details previously [13,25]. Briefly, before modification with urea or melamine, subsamples of carbons were oxidized with 50% HNO_3 for 4 h and then washed out with water to remove an excess of acid and water-soluble products of oxidation. Then the initial and oxidized samples were treated with the urea or melamine suspension in ethanol and stirred at room temperature for 5 h. The impregnated samples were heated in nitrogen at 10 °C/min to 950 °C, and maintained at these temperatures for 0.5 h. After modifications, the samples were washed with boiling water to remove any excess of urea or melamine decomposition products. The carbons after treatment are referred to as B and the modified carbons have either letter U or M added to their names, representing urea or melamine, respectively. The preoxidized samples are referred to with the letter O. Thus, for example, the B–MO is BAX-1500 preoxidized, treated with melamine and heated at 950 °C.

2.2. Methods

2.2.1. Elemental analysis—*CHN*. The content of carbon, hydrogen and nitrogen was evaluated in commercial Schwarzkopf lab, New York, NY.

The content of phosphoruswas obtained using ICP method.

2.2.2. XPS—The XPS measurements were performed on ESCALAB220i-XL (VG Scientific, UK) using monochromated Al Kα excitation source. The survey and high-resolution spectra were collected with the 100 eV and 20 eV pass energy, respectively. The quantitative analysis was done with CASAXPS software after Shirley background subtraction. The best peak fits were obtained using mixed 30% Gaussian–Lorentzian line shapes at the same FWHM for all fitted peaks.

2.2.3. Nuclear magnetic resonance (NMR)—The samples were studied using ^{31}P magic-angle spinning nuclear magnetic resonance (MAS NMR) spectroscopy. Measurements were performed on a Varian-S spectrometer operating at 122 MHz (^{31}P Larmor frequency) and spinning frequency of 22 kHz. NMR-ready samples were prepared under ambient lab conditions by packing as-given or minimally ground powders into 3.2 mm thick wall rotors. Free-induction decays (FIDs) were obtained using a phase cycled $\pi/2$ *pulse – acquire – recycle delay* sequence, and spectra were gathered by Fourier transformation of the FIDs. We used $\pi/2$ pulse widths of 3.25 μs and recycle delays of 1 s. Depending on the sample, 12 k to 60 k FIDs were signal averaged before processing. The spectral frequency scale, as given in the normalized units of ppm, is relative to the ^{31}P chemical shift of 85% H_3PO_4.

2.2.4. Electrochemical measurements—The capacitive performance of carbon samples was investigated in 1 M H_2SO_4 using a 2-electrode testing cell. The working electrode was prepared by mixing the carbon (vacuum-dried at 200 °C for 6 h) with polyvinylidene fluoride (PVDF) and commercial Mitsubishi carbon black (8:1:1) in N-methyl- 2-pyrrolidone (NMP) until homogeneous slurry. The slurry was coated on a Ti foil (current collector) with the total surface area of 1 cm^2 of an active material. The electrodes were dried at 150 ° C for 1 h and then weighted. The total mass was between 3 and 7 mg and two electrodes with identical or very close weight were selected for the measurements. Each cell was evacuated before electrolyte insertion to remove the excess of air/oxygen. In addition, the insertion of electrolyte under vacuum improved the wetability of the electrodes.

The galvanostatic charge–discharge was used in specific capacitance calculations. The measurements were carried out using Solartron 1480 Multistat within the cell voltage window of 1 V and the current loads of 50 mA/g, 100 mA/g, 0.5 A/g and 1 A/g. The specific gravimetric capacitances of cells (C) were calculated from the discharge curves according to the Eq. (1):

$$C = I \times \Delta t / \Delta U \quad (1)$$

where I (A/g) is the current load; Δt (s) is the discharge time and ΔU (V) is the cell voltage window. The published gravimetric capacitances of carbon samples are usually presented as the specific gravimetric capacitance per one electrode, i.e. the capacitance of a 3-electrode cell. Therefore in order to compare performance of our samples with the already reported values, the capacitances were calculated per one electrode (C_g), i.e. the C from 2-electrode were multiplied by 4 [26].

3. Results and discussion

The elemental composition of bulk carbon and its surface composition (XPS data) are summarized in Table 1.

Although the majority of XPS data has been reported previously in details in reference [13] along with the original deconvoluted spectra, for the purpose of this study it is important to look at the surface composition of carbons in the context of the phosphorus content, which has not been studied in details. It is clear that the incorporation of a vast quantity of oxygen-containing acidic groups at oxidation makes the phosphorus less visible. The surface phosphorus content decreases from 0.7% to only 0.1% (in terms of atomic%). However, after the urea and/or melamine treatments, which certainly result in the decomposition of a significant number of oxygen containing groups in the case of preoxidized samples, the amount of surface phosphorus atoms increases. Nevertheless, it does not return to the original values owing to the formation of nitrogen functionalities. It should be noted here that with the incorporation of nitrogen not only the content of oxygen decreases but also much less hydrogen

is present. This is the result of a higher degree of aromatization of the heat-treated carbons compared to the original B sample, which was manufactured at about 600 °C. Volatization of some organic matter upon heat treatment results also in an apparent increase in the phosphorus content. It is interesting that with an increase in the content of nitrogen in the preoxidized samples the content of hydrogen also increases, with the greater effect for the melamine treated sample, B–MO than for B–UO. Taking into account the proposed mechanism of carbonization addressed in details (reactions) in Ref. [13] and the thermal transformations of the nitrogen containing species into the predominantly quaternary and pyridinic nitrogen [19], the hydrogen should be associated mainly with oxygen or phosphorus functionalities. While the association with oxygen after heating at high temperature could be linked to basic species, the association with phosphorus, in the protonated pyrophosphate species, $HPO_3O_{1/2}^-$ or $H_2PO_3O_{1/2}$ would rather increase the acidity. Taking into account the low phosphorus content, its effect on acidity should be rather local. Even though the trend in the amount of phosphorus is detected by both methods only about 1/3 of the total phosphorus is seen on the surface. This calculation was based on the percentage of atoms from XPS and the atomic mass of phosphorus.

The XPS results as weighted concentration of oxygen and nitrogen species are presented in Table 2. They are calculated by multiplying relative concentrations in atomic% by the total atomic content of either nitrogen or oxygen. This data treatment was done to account for different amounts of surface species in each case. It should be stressed here that the amounts of surface phosphorus were too low to deconvolute the high-resolution P2p peaks.

As proposed elsewhere [13], in the case of oxygen the O-I, O-II, and O-III represent C=O groups, C–OH groups and/or C–O–C groups, and chemisorbed oxygen (carboxylic groups) and/or water, respectively with corresponding binding energies are 531 eV, 532 eV, and 535 eV. Taking into account the presence of phosphorus in all carbons under the study, O-I and O-II entities also cover the contributions from non-bridging oxygen bonded to phosphorus P=O and bridging oxygen, C–O–P, of phosphates [27,28].

In the case of nitrogen, weighted surface concentrations of pyridinic (N-6), pyrrolic/pyridone (N-5), quaternary (N–Q) nitrogen, and pyridine-N-oxide (N–X) are calculated from the peaks with the binding energies of 398 eV, 400 eV, 401 eV, and 403 eV, respectively [19–21]. The B–O contains also 2.2% of all nitrogen in the form of nitric oxides (nitro-type complexes NO_2^-) with high binding energy of 406.5 eV and nitrate $-NO_3^-$ 3 at 408 eV [29,30]. The phosphorus bonded to nitrogen is reflected in the peaks at 398 eV and 401 eV that correspond to P=N and P–N bonds, respectively [30].

As seen from the data presented, the treatment with melamine resulted in an incorporation of 20–30% more nitrogen containing groups than in the case of urea treatment with significant differences in quaternary nitrogen and pyridine-N-oxide. Moreover, the former species are the preferred groups formed either from urea or melamine precursors when the carbons are preoxidized, which is in agreement with observation of Kelemen and co-workers [31]. Preoxidation of the melamine modified samples results also in much more phenolic and/or C–O–C and carboxylic groups (water) than in the sample without preoxidation. That effect is much less pronounced for the urea modified samples where mainly O-III representing carboxylic groups and water increased for the preoxidized sample. The presence of these groups can explain the difference in the content of hydrogen.

^{31}P MAS NMR spectra are shown in Fig. 1. The only interaction represented in the spectra is that due to chemical shift isotropy (all other relevant interactions are “averaged out” from MAS); therefore, the line shapes strictly demonstrate the phosphorous site heterogeneity within each sample. The ^{31}P spectra can be generally described in terms of two features: a narrow component and a broad component, which can be separated via simulation. As is often the case

for MAS lineshapes, it is found that the narrow features are best simulated using Lorentzian–Gaussian convolution (Voight) line-shapes, Γ(x):

$$\Gamma(x)=\frac{A}{\sigma\sqrt{\pi}}\int_{-\infty}^{\infty}\frac{\exp(-f^2)}{\zeta^2+\left(\frac{x-\delta_{iso}}{\sigma}-f\right)^2}df \quad (2)$$

where *f* is the integration variable, *A* is the amplitude, σ is a width parameter and δ_{iso} is the isotropic shift or center-of-gravity (cog). The amount of Lorentzian character increases with the parameter ζ. We find that ζ = 0.54 provides a mostly Gaussian shaped peak along with a broad Lorentzian style base. The broad component, which is not well simulated by Γ(x), can be isolated through subtraction of the weighted narrow component simulation from the total spectrum. This is illustrated in Fig. 1.

Cog values and weightings were obtained for each component (Table 3). In the case of narrow component, the cogs are precisely isotropic chemical shifts and their error is small at about ±0.05 ppm. For the broad components, cogs are the average positions of phosphorus sites of large heterogeneity, and the error in these values can be as large as ±2 ppm. Weightings are integrated intensities of the normalized spectra and simply are the fraction of all phosphorus environments associated with each component. The spectral linewidth or full-width at half-maximum (FWHM) is a measure of the phosphorus site distribution within each feature. These are tabulated for each sample in Table 3.

Integrations of the ^{31}P spectra show that about 20–35% of all phosphorus atoms are represented by the narrow component (except for sample B–O). The narrow component cogs falls in the range reported for tetrahedral phosphate environments (PO_4 [32]). The shifts empirically depend on the number of covalent bonds in the tetrahedron and the degree of π-bond character. Pyrophosphate species contain 1 bridging oxygen atom and are characterized by isotropic shifts within the range of about 0 to +10 ppm. Some typical pyrophosphates include: $PO_3O^{2-}_{1/2}$, $HPO_3O^{-}_{1/2}$, $H_2PO_3O_{1/2}$. Metaphosphates have 2 bridging oxygens and are more shielded, generally occurring within the range of −20–0 ppm. Some examples of metaphosphate species include: $PO_2O^{-}_{2/2}$, $HPO_2O_{2/2}$, *n*-member chain species $P_nO_{3n-1}O^{n-}_{2/2}$, and their protonated analogs. Resonances from fully covalent phosphate species containing three bridging oxygen atoms, $POO_{3/2}$, are correspondingly shielded (perhaps as much as −40 ppm). The degrees of shielding (more negative shift) and deshielding (more positive shift) are strongly dependent on the P–O bond lengths and P–O–C (and P–O–P) bond angles. The distributions in bond lengths and angles are reflected in the FWHM. As a rough measure, FWHM values generally indicate more structural disorder amongst phosphorus environments upon modification.

Considering the B and B–O samples, the most obvious spectral difference is the absence of a narrow component for the latter. This is purely an oxidation effect and can be correlated with the dramatic reduction of surface phosphorus atoms, as shown by the XPS P data in Table 1. It is apparent that surface pyrophosphates present in sample B (at 0.43 ppm) are lost and/or converted into other subsurface phosphorus species as represented within the 11.8 ppm broad component of sample B–O. A minor peak is also found for sample B at −1.33 ppm. This contribution, which could be from surface metaphosphates is also lost or converted upon oxidation.

Note the similarity between the broad feature of sample B and the entire spectrum of sample B–O (Fig. 1). Simulation reveals two main subcomponents here: a highly deshielded component and a broad *constant* component centered at 1.2 ppm. The cog of the deshielded

component, being affected by oxidation, reduces from 14.5 ppm to 11.8 ppm and the weighting increases, due to the contribution from converted species. However, the fact that the cogs are so much more deshielded, relative to shifts of typical pyrophosphates, indicates a fundamentally different structure for these phosphorus environments. A substantial presence of P–C and P–N bonds is likely, since molecules containing these bonds typically exhibit large and positive ^{31}P shifts [33]. The *constant* component cog and weight, as described, is little affected by oxidation. On the other hand, for the B–O sample the FWHM anomalously decreases from 25 ppm to 11 ppm, which might be related to more homogenous surface phosphorus chemistry formed upon strong oxidation and the decrease in relative number of phosphorus atoms on the surface as a result of a significant increase in the oxygen atoms incorporated to the carbon matrix.

With the urea/melamine modification, the narrow component appears broader and more shielded. The presence of the peak is somewhat of a surprise for the preoxidized samples since the narrow component disappears altogether in the B–O sample. As observed with the XPS P data, upon modification of B–O to form B–UO and B–MO, there is a regeneration of surface phosphates. This phenomenon may occur as a byproduct of the high temperature processing used during the modification and decomposition of a significant number of oxygen containing functional groups. Cogs differ from those for the B and B–O samples by as much as −5 ppm for the narrow component, and −8 ppm for the broad component. In that oxygen depletion where carbon and nitrogen incorporation accompany modification, it is reasonable to assume an enhancement in both P–C and P–N bond formation. However, as mentioned above, these bonds generally yield positive ^{31}P shifts. A more plausible explanation is that upon the modification non-bridging oxygen atoms are converted into covalent bridging oxygen atoms, $P–O^{-} \rightarrow P–O–$, as in the conversion of pyrophosphate into metaphosphate species (i.e. B to B–U: $PO_3O^{2-}_{1/2} \rightarrow PO_2O_{2/2^-}$). In this way, the cog of the narrow line reflects an increasing metaphosphate character within the distribution of surface phosphates. The more pronounced negative shift for the preoxidized samples is probably due to the absence of pyrophosphates in the B–O sample. Again, as with the B and B–O samples, there is a fair correlation between the surface phosphorus content, as given by the XPS results in Table 1 and the relative weight of the narrow components.

Larger cogs are observed for B and B–O; however, the most substantial differences between them and the modified materials are with lineshapes. In that the narrow component has been identified with surface phosphates, the broad component is primarily identified with very heterogeneous subsurface phosphorus environments including phosphates and more complex structures containing multiple P–C, P–N (and P=N) bonds. These distributions are very much different between the nitrogen-containing and the initial materials. Generally, the most deshielded resonances occur with environments containing P–C bonds (around 10 ppm or more) followed by P–N bonds (around 1 ppm or more). The B and B–O samples, display a large proportion of P–C influenced environments as implied by cogs near and above 12 ppm. The most shielded resonances are found for covalent phosphates such as $PO(OP)_3$ and $PO(OC)_3$. Between the deshielded and shielded extremes occur alkyl phosphates (phosphocarbonaceous esters) containing one or two non-bridging oxygens, pyro- and meta-phosphates. The broad component gathered for the modified samples has very large distributions covering the entire range of tetrahedral phosphorus environments; however, the fairly large cogs around 5 ppm imply a substantial representation of alkyl phosphates and nitrided phosphorus environments. Finally, it is important to note that for the nitrogen-containing samples, cogs for both broad and narrow components reduce by about 2 ppm with preoxidation. This common difference suggests that the widespread purging of surface pyrophosphate species by oxidation prior to the high temperature modification influences the

distribution of surface phosphates (regenerated by modification) as well as the distribution of subsurface phosphorus environments.

Taking into account the above discussion on linking the cog to the chemical environment of phosphorus and the FWHM to the distribution of species, the linear trends between the FWHM of the broad component of the ^{31}P NMR spectra (BFWHM) and the contents of nitrogen and oxygen in our samples indicate their direct contribution to the phosphorous surface compounds (Fig. 2). Similar trends were founds for the narrow components FWHM (NFWHM). It is interesting that with an increase in the content of nitrogen as a result of surface modifications new types of species are formed, likely those involving P–N and P–C. Since this increase in nitrogen is accompanied by a decrease in the oxygen content and more or less constant phosphorus, it is likely that less oxygen is involved in the covalent bonds with phosphorus.

This relationship between the chemistry of nitrogen species detected using XPS and their effects on the chemical environment of phosphorus is more directly seen in Fig. 3. The most influential species on BFWHM seem to be the species identified as quaternary and pyridinic nitrogen. One has to remember that those species were identified assuming that only carbon and oxygen atoms are involved in binding with nitrogen. In fact if one takes into account phosphorus, the binding energies of phosphorus bonded to nitrogen as P=N and P–N bonds have been in the range of those for pyridinic and quaternary nitrogen as discussed above. This would explain the contribution of P–N (P=N) bonds to the heterogeneity of the phosphorus species present in the investigated samples.

The same approach can be used for reevaluation of the deconvolution of O1s spectra. As Fig. 4 shows, the most influence on the heterogeneity of the FWHM, with the opposite effects than nitrogen, have the species identified as O-I and O-II at binding energies of 531 and 532 eV that do not just correspond to C=O and C–OH/C–O–C but also to P=O and P–O–C.

In order to study the effect of phosphorus on the electrochemical capacitance, the cogs of both the narrow (Ncog) and the broad (Bcog) components are plotted against the capacitance of modified samples and the corresponding correlations are shown in Fig. 5. It is observed that deshielding of Ncog and Bcog has positive effect on the capacitance and the slope of the lines representing the linear trend for Ncog and Bcog are very similar. As discussed above, the most shielded Ncogs correspond to the surface metaphosphates and from the data shown in Table 3 it is evident that the preoxidized samples contain more of these species than their non-preoxidized counterparts. The specific capacitances of B–UO and B–MO are however lower than those of B–U and B–M whose surfaces consist of more pyrophosphates than metaphosphates. This suggests that the surface pyrophosphates have positive effect on the capacitance through some possible Faradaic interactions. Similarity between the slopes of Ncog and Bcog implies the equivalent importance of surface and subsurface phosphorus environment on the capacitive performance of the carbons under the study. In other words, surface phosphates and subsurface structures involving P–N and P=N bondings are confirmed to positively affect the capacitive performance of carbons.

Since it is established that surface texture and particularly the volume of small pores and their sizes affect the capacitance [3,6,8,13,14] the dependence of the specific capacitance recalculated per unit volume of micropores and the unit surface area (reported in Ref. [13]) are presented in Fig. 6A and B, respectively. As seen, the linear trend is found with the slopes similar to both cog groups especially for capacitance normalized per unit surface area. The negative slopes indicate a significant effect of the developed pore structure on the electrochemical performance.

Another important aspect is to look at the effect of phosphorus on the capacitance retention at higher current loads. Fig. 7 displays the relationship between the capacitance retention ratio of

the modified samples (including the B sample) and the NFWHM and BFWHM. It is evident that the surface P environment represented by NFWHM has more pronounced positive effect than the subsurface phosphorus site distribution reflected in BFWHM. A close look on the weights of the corresponding phosphorus species (Table 4) reveals that samples with dominant pyrophosphates retain less capacitance than those consisted of predominant metaphosphates. This trend is opposite to that of the role of surface phosphates on specific capacitance discussed above and displayed in Fig. 5 and Fig. 6. The largest specific capacitance of B–M with the most deshielded Ncog (−2.47 ppm) among the treated samples corresponding to pyrophosphates can be explained on the basis of these conclusions. In addition, the lowest capacitance retention of B–M at the current load of 1 A/g is in good agreement with its highest fraction of pyrophosphates reflected in largest weight (0.27) among the treated samples.

In the light of these observations, it is anticipated that activated carbons with higher content of phosphorus will exhibit enhanced capacitive performance in acidic electrolyte. In addition, this initial study confirmed that both the specific capacitance and capacitance retentions can be influenced by controlling the phosphorus environment.

4. Conclusions

The results presented in this paper show that presence of phosphorus in a small but measurable quantity in the carbon matrix has a considerable effect on the electrochemical performance. Formations of phosphorus–nitrogen and phosphorus–carbon bonds, accompanied with the decrease in bridging oxygen and the numbers of phosphates, increase the heterogeneity of the carbon surface and result in compounds which have positive effects on the overall capacitance and on the improvement of the capacitance retention ratio.

REFERENCES

1. Simon P, Gogotsi Y. Materials for electrochemical capacitors. Nat Mater 2008;7:845–854. [PubMed: 18956000]
2. Pandolfo AG, Hollenkamp AF. Carbon properties and their role in supercapacitors. J Power Sources 2006;157:11–27.
3. Chmiola J, Yushin G, Gogotsi Y, Portet C, Simon P, Taberna PL. Anomalous increase in carbon capacitance at pore size below 1 nm. Science 2006;313:1760–1763. [PubMed: 16917025]
4. Huang J, Sumpter BG, Meunier V. Theoretical model for nanoporous carbon supercapacitors. Angew Chem Int Ed 2008;47:520–524.
5. Largeot C, Portet C, Chmiola J, Taberna PL, Gogotsi Y, Simon P. Relation between the ion size and pore size for an electric double-layer capacitor. J Am Chem Soc 2008;130:2730–2731. [PubMed: 18257568]
6. Raymundo-Piñero E, Kierzek K, Machnikowski J, Bèguin F. Relationship between the nanoporous texture of activated carbons and their capacitance properties in different electrolytes. Carbon 2006;44:2498–2507.
7. Salitra G, Soffer A, Eliad L, Cohen Y, Aurbach D. Carbon electrodes for double-layer capacitors. I. Relations between ion and pore dimensions. J Electrochem Soc 2000;147:2486–2493.
8. Chmiola J, Dash R, Yushin G, Gogotsi Y. Effect of pore size and surface area of carbide derived carbon on specific capacitance. J Power Sources 2006;158:765–772.
9. Marsh, H.; Rodíguez-Reinoso, F. Activated carbon. Oxford, San Diego: Elsevier; 2006.
10. Boehm, HP. Advances in catalysis. Vol. vol. 16. New York: Academic Press; 1966. Chemical identification of surface groups; p. 179-274.
11. Andreas HA, Conway BE. Examination of the double-layer capacitance of an high specific-area C-cloth electrode as titrated from acidic to alkaline pHs. Electrochim Acta 2006;51:6510–6520.
12. Montes Moran MA, Suarez D, Menendez JA, Fuente E. On the nature of basic sites on carbon surfaces: an overview. Carbon 2004;42:1219–1225.

13. Seredych M, Hulicova-Jurcakova D, Lu GQ, Bandosz TJ. Surface functional groups of carbons and the effects of their chemical character, density and accessibility to ions on electrochemical performance. Carbon 2008;46:1475–1488.
14. Hulicova-Jurcakova D, Seredych M, Lu GQ, Bandosz TJ. Combined effect of nitrogen- and oxygen-containing functional groups of microporous activated carbon on its electrochemical performance in supercapacitors. Adv Funct Mater 2008;18:1–10.
15. Adib F, Bagreev A, Bandosz T. Adsorption/oxidation of hydrogen sulfide on nitrogen-containing activated carbons. Langmuir 2000;16:1980–1986.
16. Bèguin F, Szostak K, Lota G, Frackowiak E. A self-supporting electrode for supercapacitors prepared by one-step pyrolysis of carbon nanotube/polyacrylonitrile blends. Adv Mater 2005;17:2380–2384.
17. Hulicova D, Kodama M, Hatori H. Electrochemical performance of nitrogen-enriched carbons in aqueous and non-aqueous supercapacitors. Chem Mater 2006;18:2318–2326.
18. Kodama M, Yamashita J, Soneda Y, Hatori H, Kamegawa K. Preparation and electrochemical characteristics of N-enriched carbon foam. Carbon 2007;45:1105–1107.
19. Pels JR, Kapteijn F, Moulijn JA, Zhu Q, Thomas KM. Evolution of nitrogen functionalities in carbonaceous materials during pyrolysis. Carbon 1995;33:1641–1653.
20. Jansen RJJ, van Bekkum H. XPS of nitrogen-containing functional groups on activated carbon. Carbon 1995;33:1021–1027.
21. Raymundo-Piñero E, Cazorla-Amorós D, Linares-Solano A, Find J, Wild U, Schlögl R. Structural characterization of N-containing activated carbon fibers prepared from a low softening point petroleum pitch and a melamine resin. Carbon 2002;40:597–608.
22. Frackowiak E, Lota G, Machnikowski J, Vix-Guterl C, Bèguin F. Optimisation of supercapacitors using carbons with controlled nanotexture and nitrogen content. Electrochim Acta 2006;51:2209–2214.
23. Puziy AM, Poddubnaya OI, Martínez-Alonso A, Suárez-García F, Tascón JMD. Synthetic carbons activated with phosphoric acid: I. Surface chemistry and ion binding properties. Carbon 2002;40:1493–1505.
24. Jagtoyen M, Derbyshire F. Activated carbons from yellow poplar and white oak by H_3PO_4 activation. Carbon 1998;36:1085–1097.
25. Seredych M, Bandosz TJ. Desulfurization of digester gas on wood-based activated carbons modified with nitrogen: Importance of surface chemistry. Energy Fuels 2008;22:850–859.
26. Qu D, Shi H. Studies of activated carbons used in double-layer capacitors. J Power Sources 1998;74:99–107.
27. Puziy AM, Poddubnaya OI, Socha RP, Gurgul J, Wisniewski M. XPS and NMR studies of phosphoric acid activated carbons. Carbon 2008;46:2113–2123.
28. Lee TH, Jolly WL, Bakke AA, Weiss R, Verkade JG. On correlating phosphorus core binding energies, phosphorus lone pair ionization potentials, and proton affinities of tervalent phosphorus compounds. J Am Chem Soc 1980;102:2631–2636.
29. Marchand R, Agliz D, Boukbir L, Quemerais A. Characterization of nitrogen containing phosphate glasses by X-ray photoelectron spectroscopy. J Non-Cryst Solids 1988;103:35–44.
30. Perry WB, Schaaf TF. An X-ray photoelectron spectroscopic study of charge distributions in tetracovalent compounds of nitrogen and phosphorus. J Am Chem Soc 1975;97:4899–4905.
31. Kelemen SR, Gorbaty ML, Kwiatek PJ. Quantification of nitrogen forms in Argonne premium coals. Energy Fuels 1994;8:896–906.
32. Duncan TM, Douglas DC. On The 31P chemical shift anisotropy in condensed phosphates. Chem Phys 1984;87:339–349.
33. Gorenstein, DG. Phosphorus-31 NMR principles and applications. New York: Academic Press; 1984.

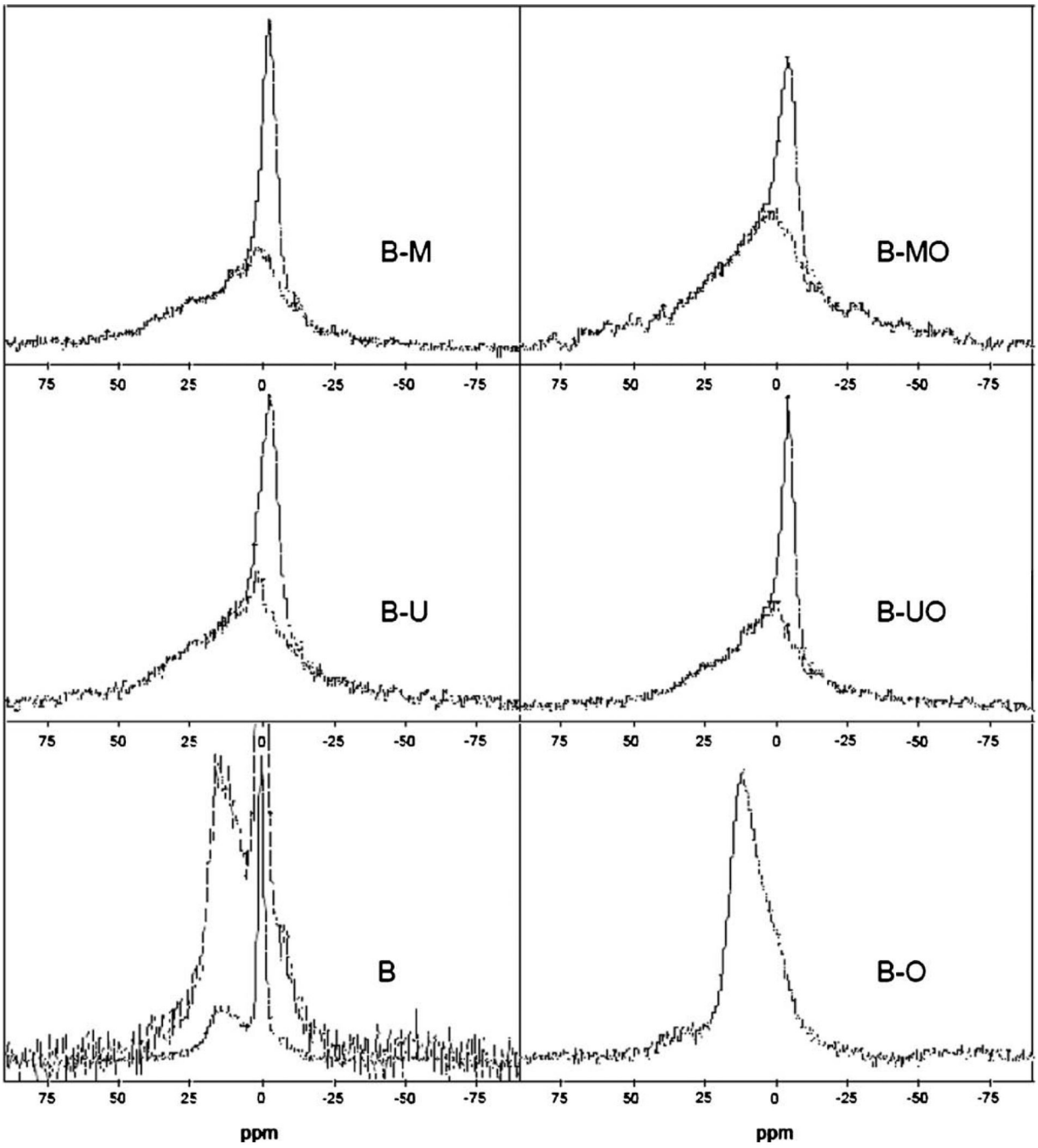

Fig. 1.

^{31}P MAS NMR spectra for carbon samples under the study. The broad component in the spectrum of sample B is also magnified in order to show similarities with that of sample B–O. The broad components are shown for modified samples (B–U, B–UO, B–M and B–MO) by the extended dashed lines under the narrow features.

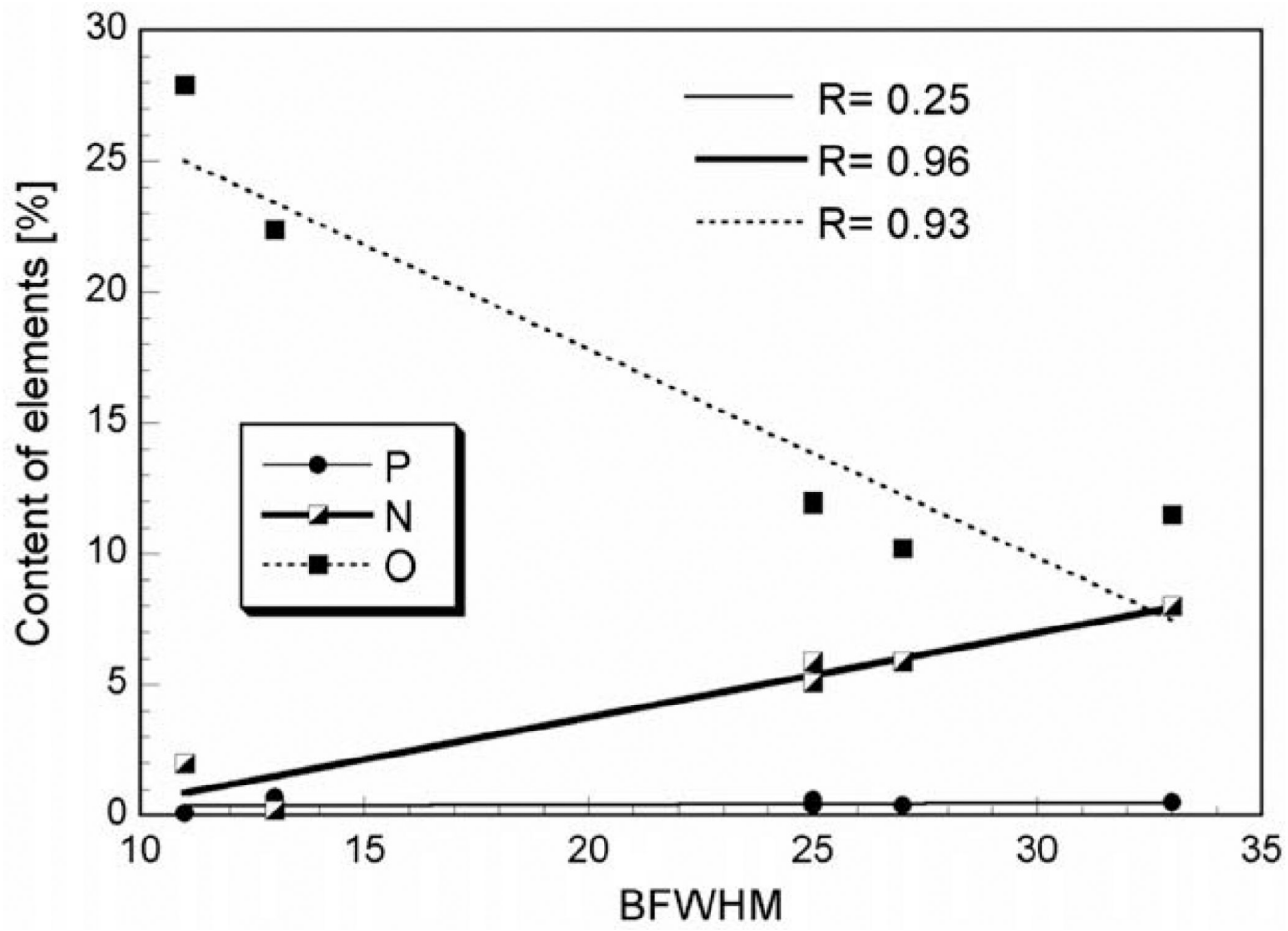

Fig. 2.
Relationship between the content of heteroatoms in carbons and FWHM of the broad components of the ^{31}PMAS NMR spectra.

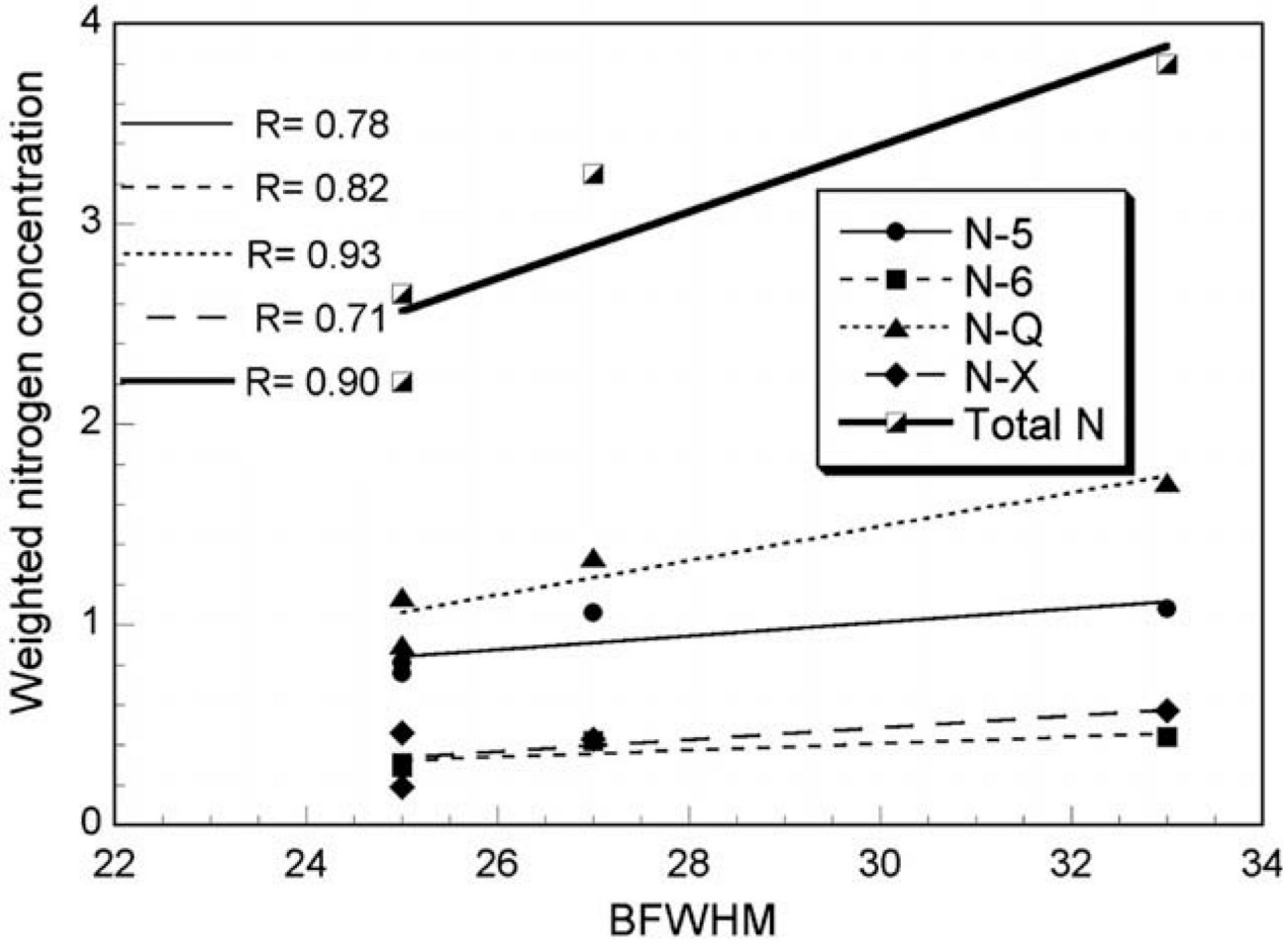

Fig. 3.
Relationship between weighted nitrogen concentrations of species detected from XPS analysis and FWHM of the broad components of the ^{31}P MAS NMR spectra.

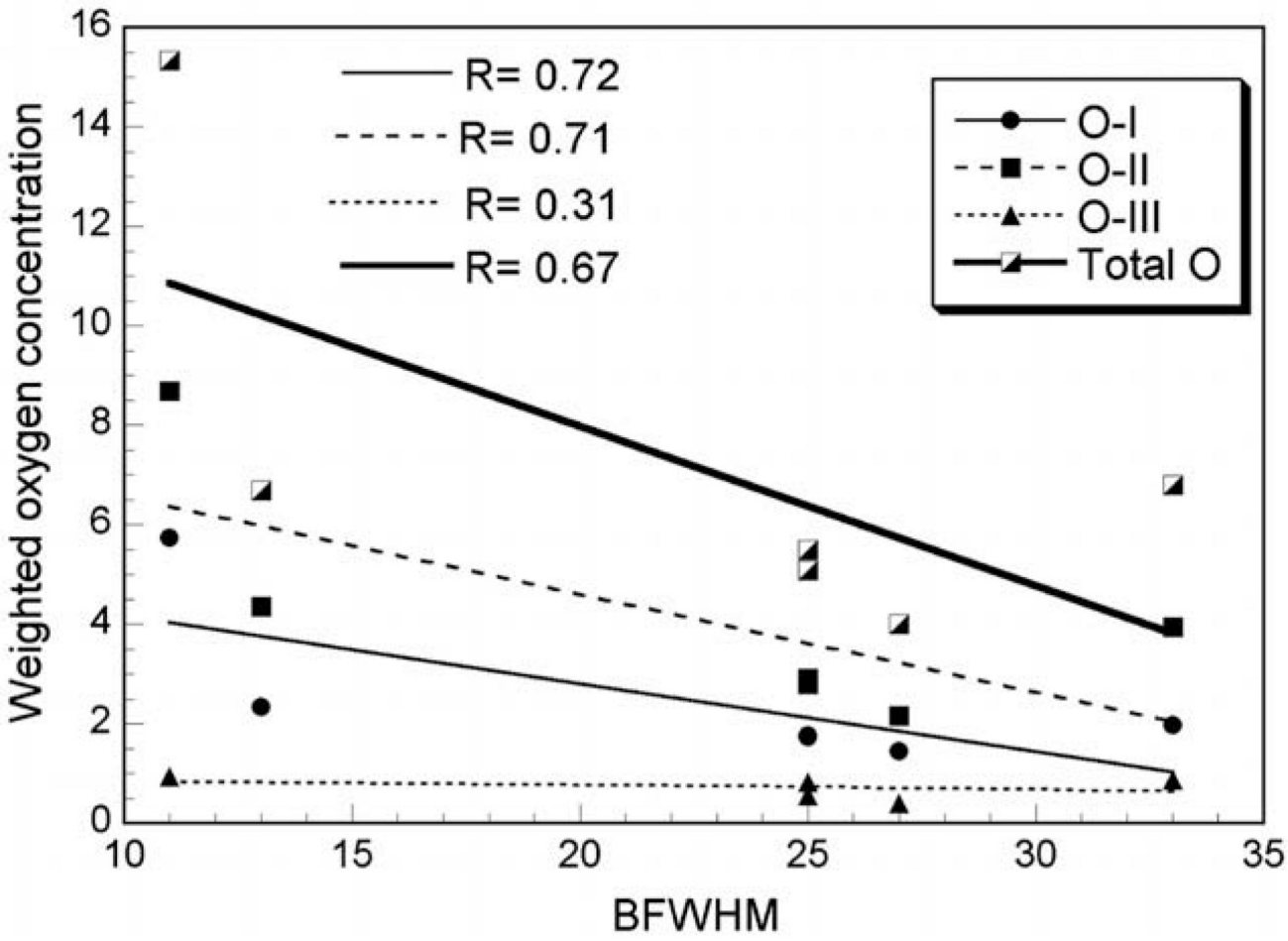

Fig. 4.
Relationship between the weighted oxygen concentrations of species detected from XPS analysis and the FWHM of the broad components of the ^{31}P MAS NMR spectra.

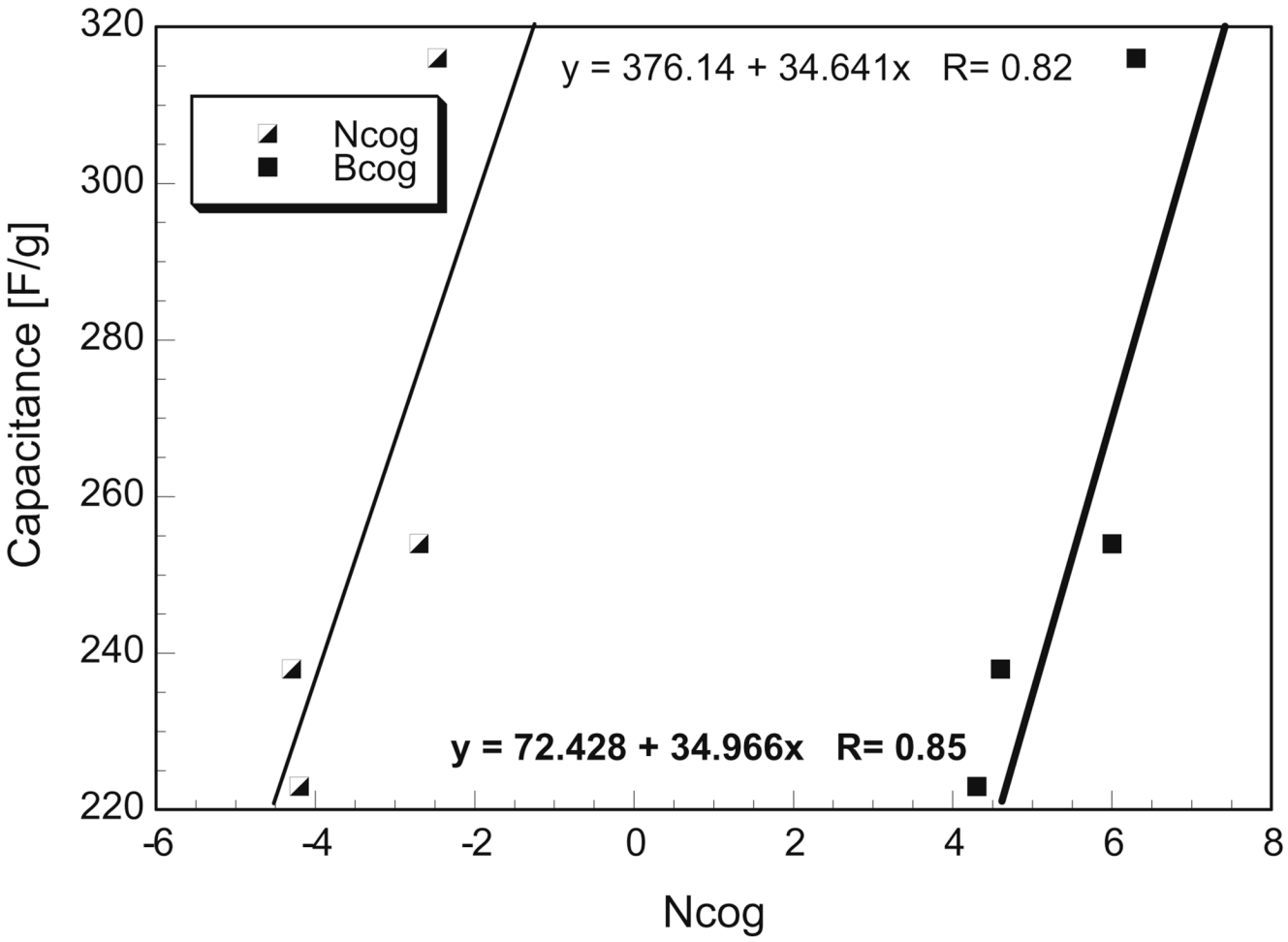

Fig. 5.
Relationship between the electrochemical capacitance and cogs of both components of the ^{31}P MAS NMR spectra for the carbons modified with nitrogen.

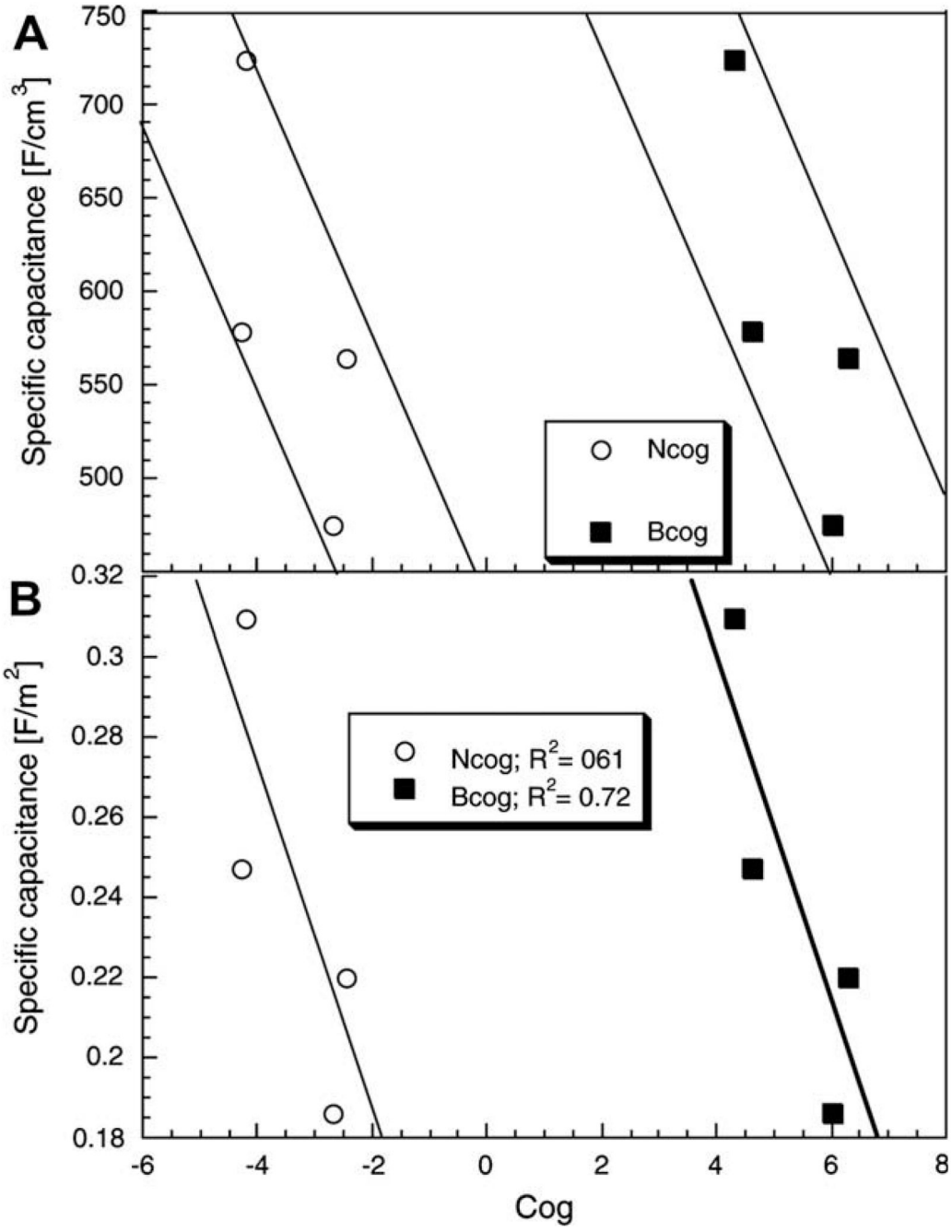

Fig. 6.

Relationship between the specific electrochemical capacitance, in F/cm^3 (A) and in F/m^2, and cogs of both components of the ^{31}P MAS NMR spectra for the carbons modified with nitrogen (B).

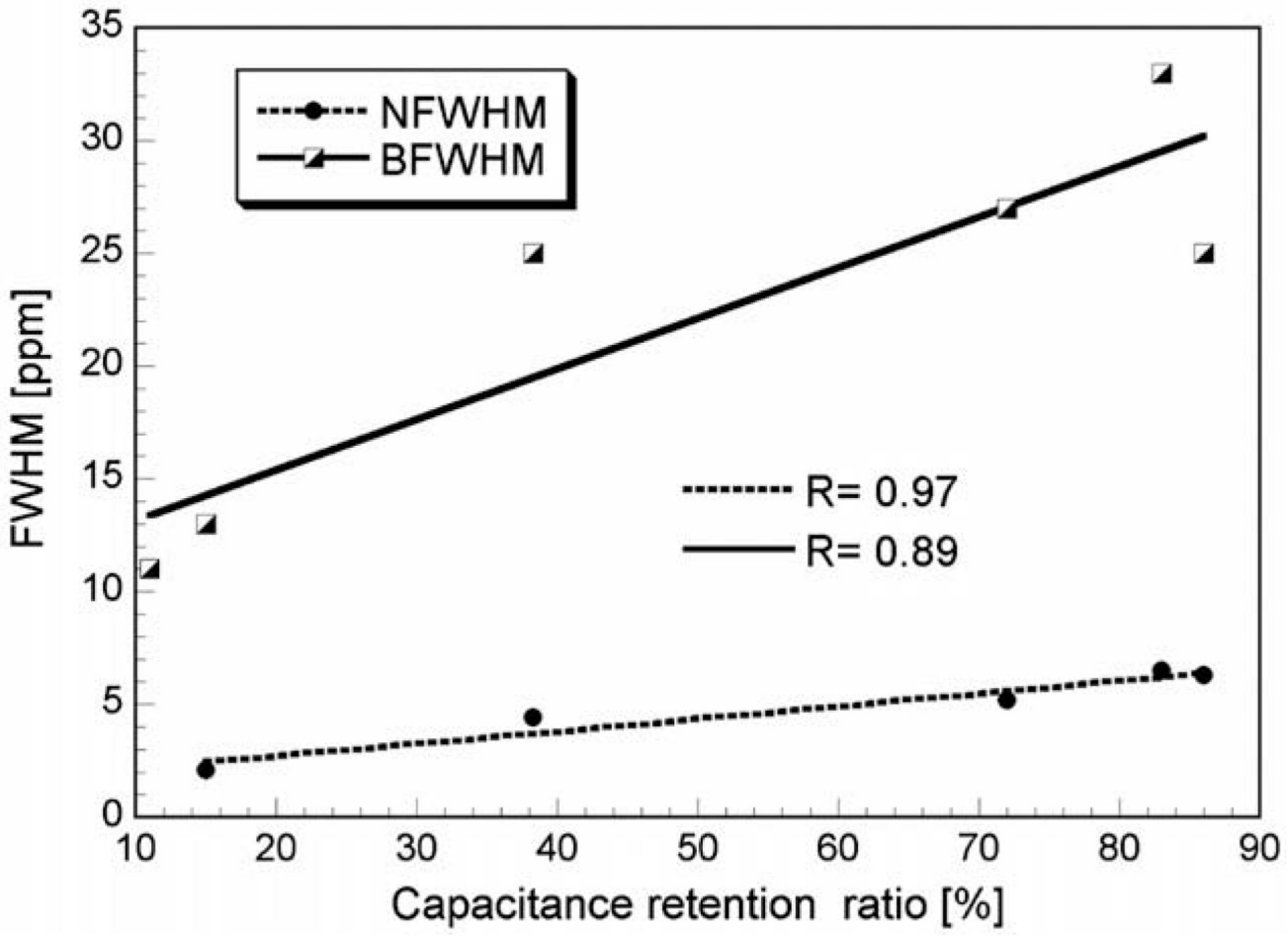

Fig. 7.

Relationship between the FWHM of both components of the ^{31}P MAS NMR spectra and the capacitance retention ratio. The retention ratios for B, B–O, B–U, B–UO, B–M, B–MO are 15%, 11%, 86%, 86%, 72%, and 83%, respectively. The ratios were obtained by dividing the capacitance at the current load of 1000 mA/g by the capacitance at 50 mA/g (100 mA/g in the case of B–O) [13].

Table 1

Carbon, hydrogen, nitrogen, phosphorus, and oxygen contents in the samples studies [13].

	Elemental analysis (%)						XPS[a]			
Sample	**C**	**H**	**N**	**O + P**	$\sqrt{P}$[b]	**N/C**	**C**	**O**	**N**	**P**
B	73.8	3.6	0.2	22.4	0.58	0.003	91.4	6.7	–	0.7
B–O	68.2	2.1	2.0	27.9	0.17	0.03	82.2	15.5	2.2	0.1
B–U	82.2	0.7	5.1	12.0	0.67	0.06	90.0	5.1	3.1	0.6
B–UO	81.4	0.8	5.9	11.9	0.43	0.07	89.7	5.5	3.8	0.4
B–M	83.3	0.6	5.9	10.2	0.60	0.07	89.6	4.0	4.8	0.4
B–MO	79.6	0.9	8.0	11.5	0.41	0.10	86.5	6.8	5.7	0.5

[a] Percentage of atoms on the surface (mol%).

[b] From ICP.

Table 2

Weighted surface concentrations of nitrogen and oxygen species obtained by fitting the N1s and O1s core level peaks of XPS spectra.

Sample	N-5	N-6	N–Q	N–X	O-1	O-II	O-III
B	–	–	–	–	2.34	4.35	–
B–O	–	–	–	–	5.73	8.68	0.93
B–U	0.81	0.31	0.90	0.19	1.73	2.80	0.56
B–UO	0.76	0.29	1.14	0.46	1.76	2.91	0.82
B–M	1.06	0.42	1.34	0.43	1.44	2.16	0.40
B–MO	1.08	0.44	1.71	0.57	1.97	3.94	0.88

Carbon N Y. Author manuscript; available in PMC 2010 March 29.

Table 3

Results on ^{31}P MAS NMR analysis.

Sample	Narrow component[a]			Broad component[b]		
	Cog(ppm)	Weight	FWHM(ppm)	Cog(ppm)	Weight	FWHM(ppm)
B	0.43	0.35	2.1	14.5	0.33	13
	−1.33	0.02	1.4	1.2	0.30	25
B–O	–	–	–	11.8	0.70	11
				1.2	0.30	11
B–U	−2.70	0.25	6.3	6.0	0.75	25
B–UO	−4.30	0.24	4.4	4.6	0.76	25
B–M	−2.47	0.27	5.2	6.3	0.73	27
B–MO	−4.20	0.19	6.5	4.3	0.81	33

[a] Narrow component error = ±0.05 ppm.

[b] Broad component error = ±2 ppm.

Table 4

Gravimetric capacitances C_g, and the capacitance retention ratios R_{Cg} of original and modified carbons.

Sample	C_g at 100 mA/g (F/g)	R_{Cg} (%)
B	208	15
B–O	105	11
B–U	254	86
B–UO	238	86
B–M	316	72
B–MO	223	83